J Sol-Gel Sci Technol (2015) 76:542–551
DOI 10.1007/s10971-015-3804-3

ORIGINAL PAPER

Novel organic–inorganic hybrid materials based on epoxy-functionalized silanes

Manatchanok Sitthiracha[1,2] · Paul Andrew Kilmartin[1,2] · Neil Raymond Edmonds[1,2]

Received: 14 November 2014 / Accepted: 6 July 2015 / Published online: 22 July 2015

Abstract Hybrid materials comprising inorganic glasses and organic polymers were investigated as potential replacements for diglycidyl ether of bisphenol-A to improve the thermomechanical properties of available composites. An epoxy-functionalized silane, 3-glycidoxypropyltrimethoxysilane (GPTMS), was employed to synthesize organic–inorganic hybrid materials (OIHMs) via a sol–gel process. The oxirane ring in GPTMS was cross-linked by compounds including an aliphatic amine, diethylenetriamine, amine-functionalized silane, n-(2-aminoethyl)-3-aminopropyltrimethoxysilane, tertiary amine, 2,4,6-tris(dimethylaminomethyl)phenol (DMP-30), and an acid anhydride, hexahydrophthalic anhydride. OIHMs derived from a difunctional organosilane, (3-glycidoxypropyl)methyldimethoxysilane, were also synthesized to compare the mechanical properties with OIHMs derived from GPTMS. Structural characterization of cured OIHMs was performed using a combination of attenuated total reflectance spectroscopy (FTIR-ATR) and ^{29}Si solid-state nuclear magnetic resonance. Differential scanning calorimetry and thermogravimetric analysis were used to clarify the thermal properties. The thermomechanical properties and cross-link density were evaluated using dynamic mechanical thermal analysis (DMTA). In this study, it was evident that the presence of inorganic networks provided a significant improvement of the thermomechanical properties, where the glass transition temperature typically increases by 20 °C and the storage modulus at 150 °C by nearly eight times that of neat epoxy resin. An increase in glass transition temperature, end-use temperature, and the thermomechanical behavior of OIHMs was observed and quantified using DMTA. These results corresponded to calculated increases in cross-link density.

Keywords Mechanical properties · Thermal stability · Hybrid materials · Sol–gel · 3-Glycidoxypropyltrimethoxysilane · Glass transition temperature

1 Introduction

Reinforced composite materials can be found in a very wide range of applications. The diglycidyl ether of bisphenol-A (DGEBA) is by far the most commercially important epoxy resin used to form a polymer matrix. Curing of epoxides can be carried out using a variety of curing agents; however, an amine system is the most widely used curing agent due to the better understanding/control of epoxy–amine reaction [1].

In amorphous polymers, the glass transition temperature (T_g) is generally considered to be the most significant parameter in engineering applications. T_g is used to determine the mechanical properties as a function of the temperature of the material; thus, it represents the maximum use temperature. In the glassy state below T_g, it is better for the matrix to transfer load to the fiber, providing support against fiber buckling and maintaining alignment of the fibers. When operating above the glass transition temperature, the matrix becomes soft and does not perform

✉ Manatchanok Sitthiracha
m.sitthiracha@hotmail.com

[1] School of Chemical Sciences, Faculty of Science, The University of Auckland, Auckland, New Zealand

[2] Centre of Advanced Composite Materials, Faculty of Engineering, The University of Auckland, Auckland, New Zealand

well [2]. Therefore, the applications of polymer resins, for example, epoxies, vinyl esters, and unsaturated polyesters, are often restricted by their low service temperature (70–80 °C) [3].

In applications such as aviation and space domains, polymer resins with high T_g are required for high-temperature-performance composite materials. A group of resins, which can be either thermosetting or thermoplastic, are known as thermostable resins. These can be divided into two classes: bismaleimide resins (200 °C class) and polyimides (300 °C class). Even though these thermoresins offer better thermal stability than common resin systems, they are generally expensive, and their chemistry is more complex [4, 5].

It has been previously reported that OIHMs exhibit excellent mechanical properties at temperatures extending far above the T_g of the corresponding organic polymers [6, 7]. Thus, OIHMs have the potential to be used as matrix resins in polymer-reinforced composites by replacing epoxy resins with OIHMs containing epoxy as the organic component.

One of the most highly studied organically modified silanes, or so-called silane coupling agent, is 3-glycidoxypropyltrimethoxysilane (GPTMS), in which a baring epoxy ring can be opened and cross-linked with a curing agent in a similar way to the chemistry of epoxy resins. A large number of studies have been dedicated to the synthesis of organic–inorganic coatings using different silane coupling agents and reaction strategies [8–20]. Up until now, not many articles have been published on the synthesis and characterization of OIHMs derived from GPTMS silane precursors in bulk form [21, 22]. Moreover, very few papers have reported the study of OHMs as a polymer matrix in fiber-reinforced composites [23]. For OIHMs to be used as polymer matrices in such composites, a better understanding of their mechanical properties is required. However, these mechanical properties are difficult to evaluate and generalize as they vary with processing parameters, micro- and nanostructures, and the nature and extent of the organic–inorganic interfaces [22, 24]. The study of the mechanical properties of OIHMs using different techniques has become the main focus of OIHM development.

So far, measuring the mechanical properties of the coating films is commonly carried out by indentation testing on a nanometer scale, commonly referred to as nanoindentation, combined with scratch testing [25]. For bulk hybrid polymers, the resonance method and Knoop microindentation were employed. Resonance vibration measures flexural modulus as a function of resonant frequency, while elastic modulus is calculated from the results of Young's modulus measured by Knoop microindentation. Although the mechanical properties of thin coating films [26] and bulk hybrid polymers have been well established using these techniques, the evaluation of thermomechanical properties of OIHMs still remains a challenge as the T_g cannot be measured. Differential scanning calorimetry (DSC) has also been employed to evaluate the T_g of OIHMs [21, 27]. However, for highly cross-linked polymers, T_g is generally less prominent than for linear amorphous polymers. Therefore, the T_g may be difficult to observe using DSC, because the change in heat capacity (ΔC_p) will be small and occurs over a broad temperature range. The T_g of these materials may be observed more clearly with dynamic mechanical thermal analysis (DMTA) due to much larger baseline shift of storage modulus ($\Delta E'$) than the ΔC_p measured in DSC at T_g [28]. For this reason, DMTA is the main technique used to characterize the elastic behavior of various polymer-oxide hybrid materials.

2 Experimental

2.1 Material preparation

The OIHMs were synthesized via a sol–gel process, in which the GPTMS or GPDMS was hydrolyzed with a stoichiometric amount of water relative to the methoxyl groups from the silane precursor. The solution was vigorously stirred for 2 h at ambient temperature. The pH of the solution was adjusted to 2 by adding 1 M HCl. A curing agent was then added to the sol solution, and the stirring continued for an additional 5 min. The sol solution was then transferred onto a glass plate covered by a Teflon fabric and dried as bulk. All samples are listed in Table 1. For AEATPMS curing agent, the hydrolysis reaction was undertaken without adding acid catalyst as the hydrolysis of AEAPTMS is self-catalyzed due to the alkalinity of the silane compound. In the case of HHPA, the epoxy ring-opening reaction proceeds through an esterification reaction. This results in the creation of another hydroxyl group which can react with another anhydride group through a similar esterification. In the presence of free acid groups acting as catalysts, the generated hydroxyl group reacts with another epoxy ring to form an ether linkage. This reaction, although much slower than the esterification reaction at elevated temperatures, accounts for the optimum mix ratios generally being less than the stoichiometric equivalents. Therefore, the amount of anhydride needs to be reduced by half of stoichiometry to avoid residual anhydride in the product [29].

After gel formation, reactive silanol groups are still in the system as both hydrolysis and condensation are not completed. Thus, heating at relatively high temperature (above 100 °C) is required to accelerate the gel

Table 1 Sample preparation and composition of the organic–inorganic hybrid materials (OIHMs)

Sample	Curing at 100 °C (h)	Post-curing at 150 °C (h)
GPTMS/DETA (mol ratio = 1:1)	24	4
GPDMS/DETA (mol ratio = 1:1)	24	4
GPTMS/AEAPTMS (mol ratio = 1:1)	24	4
GPTMS/DMP-30 (95:5 %w/w)	24	24
GPTMS/HHPA (mol ratio = 1:0.5)	24	24
GPDMS/HHPA (mol ratio = 1:0.5)	24	24

densification by removing water, alcohol, and other volatile components [30]. In this study, all wet gels were dried at 100 °C for 24 h followed by post-curing at 150 °C. The gels derived from GPTMS/DETA, GPDMS/DETA, and GPTMS/AEAPTMS were post-cured for 4 h only, while the other gels were post-cured for 24 h. This is because the presence of unreacted amine in the wet gel decomposed or volatilized on heating at high temperature and/or for long period of time causing the change in color from yellow to dark brown. The decomposition of excess amine tends to decrease the initial decomposition temperature and mechanical properties of the cured OIHMs [31, 32].

West System® 105/207, which is a commercial standard epoxy resin and its curing agent, was chosen for property comparison with the OIHMs. The cured epoxy resin was prepared according to the manufacturer method in which the ratio of the epoxy resin to the curing agent was 5:1.

2.2 Material characterization

Cured OIHMs were characterized using a Thermo Electron Nicolet 8700 series FTIR equipped with a smart orbit ATR single-reflection accessory with diamond crystal. The infrared spectra were acquired with a resolution of 4 cm^{-1} in the spectral region from 4000 to 650 cm^{-1}. An average of 64 scans was taken for each spectrum. The measurements were taken in absorbance mode, and the spectra are presented in ATR units and linear with respect to concentration. Data acquisition and analysis were performed using standard software (Omnic ESP, version 7.1). The thermal properties of the materials were analyzed using a TA Instruments Model Q1000 calorimeter and a TA Instrument Q5000 IR TGA. Solid-state NMR measurements were taken on a Bruker 200 DRK spectrometer at a magic angle spinning (MAS) rate of 5 kHz. Thermomechanical properties of the OIHMs were evaluated using a TA Q800 DMTA in dual cantilever mode at a frequency of 1 Hz with a heating rate of 3 °C min^{-1}. The sol solution was cast onto a fiberglass veil support with the dimensions of 12 mm wide and 60 mm long to form thin films. The gel was cured as per curing regimes of the bulk OIHMs. SEM was carried out using a Philips XL30S Field Emission Gun with an energy-dispersive X-ray spectroscopy (EDS) and ultrathin window SiLi (Lithium drifted) detector.

3 Results and discussion

The derived OIHMs of GPTMS/DETA and GPTMS/AEAPTMS were found to be prone to cracking. This could be explained by the inorganic network formation in which the materials are composed to a large extent by linked clusters and have a small content of entangled linear chains as a result of two-step acid–base sol–gel process [33, 34]. For GPDMS/DETA and GPDMS/HHPA, cracking was significantly improved due to reduction in the cross-linking capability of the silane precursor (Fig. 1). Cracking was not found in GPTMS/DMP-30 even though this OIHM was synthesized under the two-step sol–gel process. This could be due to the ring-opening reaction of the tertiary amine, leading to the formation of linear chains of poly(ethylene oxide) [29, 35].

3.1 FTIR studies

In Fig. 2, the IR spectra of GPTMS/DETA and GPTMS/AEAPTMS OIHMs showed the broad absorption band at 3389 cm^{-1} assigned to an –OH stretching vibration, indicating the presence of C–OH of opened epoxy rings and Si–OH of the remaining silanol groups. In general, the Si–O–Si cage and network structure show peaks in the 1200- to 1000-cm^{-1} region, consisting of overlapping bands from the distribution of local bond types and bond angles that exist in the microstructure [36]. The formation of a siloxane network is evident from the two characteristic absorption bands at 1114 and 1043 cm^{-1}, which are assigned to the asymmetric Si–O–Si stretching mode. These two distinct bands are often ascribed to the formation of three-dimensional siloxane polymers made up of T units $[RSiO_{1.5}]_x$ [37–39]. The vibration band at 782 cm^{-1} is assigned to the Si–O–Si symmetric stretch [40]. N–H stretching vibration of secondary amine at 3281 cm^{-1} can be seen overlapping with the broad –OH stretching band. N–H in plane bending mode of secondary amine also appeared at 1459 cm^{-1}. This result suggests that some of

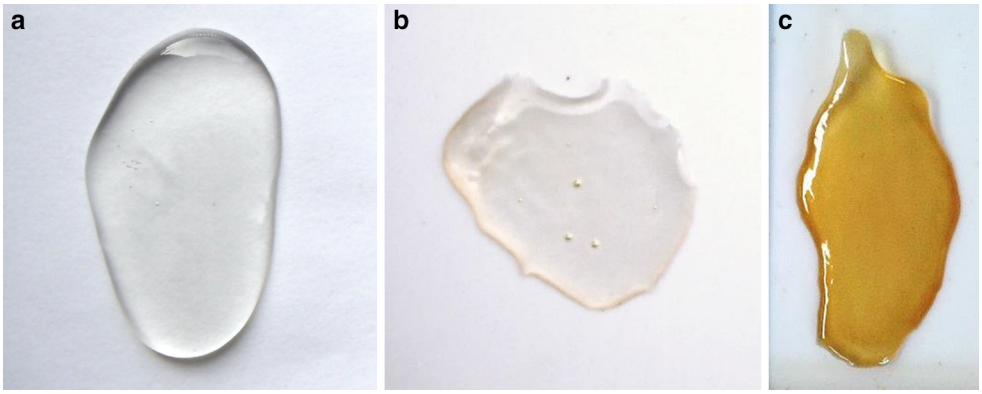

Fig. 1 OIHMs of **a** GPDMS/DETA, **b** GPDMS/HHPA, and **c** GPTMS/DMP-30

the secondary amine was not reacted and cross-linked with the epoxy ring. In respect of the presence of secondary amine, the characteristic absorptions of epoxy ring with low intensity were observed at 1251 and 855 cm^{-1}. Although the band at 3050–2955 cm^{-1} is commonly used as the characteristic absorption of epoxy ring [41–43], this peak cannot be clearly seen in all OIHM spectra. For GPTMS/DMP-30, the absorption bands corresponding to hydroxyl, ethyl, siloxane, and epoxy groups can be located at similar frequencies to those of the GPTMS/DETA hybrid material. However, the absorption bands peaking at 2871 and 930 cm^{-1} were detected due to the $–CH_3$ groups present in DMP-30 and the formed quaternary ammonium cation ($C–N^+(CH_3)_3$), respectively [44].

GPDMS/DETA showed different absorption bands for Si–O–Si, which represent the different siloxane structures (Fig. 2d). The characteristic stretching vibration modes of the linear siloxane were located at 1080, 1052, and 1018 cm^{-1}, which are similar to the absorption peaks of siloxane in polydimethylsiloxane (PDMS) [45–47]. Unlike OHIMs consisting of three-dimensional siloxane network, the formed linear siloxane chains allowed the epoxy and amine groups to react with less sterical hindrance. Hence, the corresponding bands of unreacted epoxy and amine groups were not observed. For GPTMS/HHPA, the characteristic absorptions of siloxane bonds can be seen at 1101, 1080, and 1039 cm^{-1}, indicating the mixed network structure of three-dimensional network and linear siloxane chains (Fig. 2e). This could be due to the one-step acid-catalyzed sol–gel process. The disappearance of absorptions due to symmetric and asymmetric stretching of a five-membered cyclic anhydride at 1855 and 1783 cm^{-1} confirmed that the anhydride ring-opening reaction was completed, although the epoxy rings were not fully reacted [48, 49]. From Fig. 2f, the IR spectrum of GPDMS/HHPA showed similar absorptions to that of GPTMS/HHPA. However, the absorption bands corresponding to siloxane were not as well defined as observed in GPDMS/DETA. The characteristic absorptions of epoxide group cannot be detected, which is in good agreement with the IR spectrum of GPDMS/DETA.

3.2 Thermal analyses

For GPTMS/DETA cured at ambient temperature, a step in baseline representing T_g cannot be observed (Fig. 3a). Only endothermic and exothermic peaks were observed corresponding to the evaporation of volatile species and the thermal decomposition caused by the oxidation reaction of the organic polymeric component at 325 °C, respectively [8]. The loss of well-defined T_g in the DSC curve was suggested as an indication of good molecular dispersion of organic entity in the inorganic network [50]. For GPTMS/DETA cured at 100 °C, the endothermic peak was not observed in the DSC scan, suggesting that there was little or no further curing during subsequent heating (Fig. 3b).

The results from thermal degradation studies of hybrid polymers are shown in Fig. 4, in which the temperature range was 25–600 °C. The results of TGA of these OIHMs are summarized in Table 2.

The OIHMs exhibited three distinct weight loss stages. The initial small weight loss was due to the release of absorbed moisture by the hydrophilic surface with a high surface energy. It can be seen that GPDMS/DETA and GPDMS/HHPA showed the least weight loss in the first stage, which could be explained by a low inorganic content in the material. Thus, the material absorbed a small amount of water. In contrast, GPTMS/AEAPTMS had the highest amount of absorbed water, corresponding to the high inorganic content in the material. The second stage was associated with the decomposition of the unreacted organic compounds trapped in the network [9]. The major weight loss occurred between 350 and 600 °C, which can be related to the decomposition of organic components in hybrid materials. The weight loss in this region is also believed to correspond to further condensation reactions of

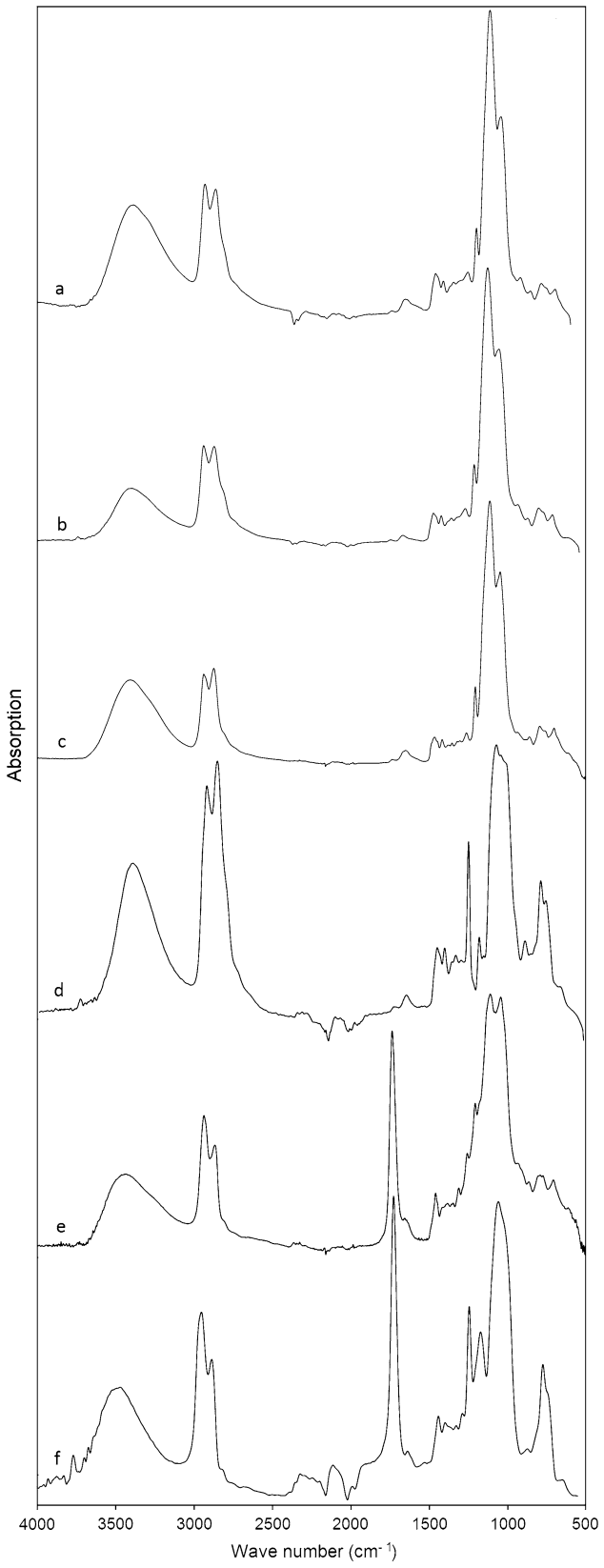

Fig. 2 FTIR spectra of *a* GPTMS/DETA, *b* GPTMS/AEAPTMS, *c* GPTMS/DMP-30, *d* GPDMS/DETA, *e* GPTMS/HHPA, and *f* GPDMS/HHPA

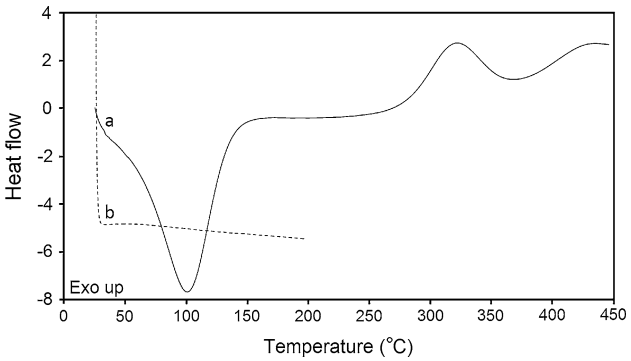

Fig. 3 DSC scan of GPTMS/DETA *a* cured at ambient temperature and *b* cured at 100 °C

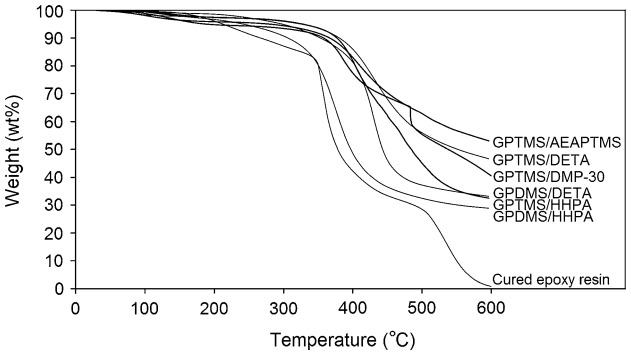

Fig. 4 TGA curves of OIHMs in comparison with the TGA curve of cured epoxy resin

Table 2 TGA of OIHMs

Weight loss (wt%)	Temperature range (°C)		
	25–150	150–350	350–600
GPTMS/DETA	3.6	5.6	60.2
GPTMS/AEAPTMS	3.7	4.7	38.6
GPTMS/DMP-30	2.2	4.2	46.9
GPDMS/DETA	1.7	4.7	61.1
GPTMS/HHPA	2.1	8.46	57.3
GPDMS/HHPA	1.1	17.6	51.1

silanol groups [51, 52]. For GPDMS/HHPA, the major weight loss occurred at the temperature around 340 °C, which is lower than that of GPTMS/HHPA and the other OIHMs derived from epoxy–amine systems. Thus, GPDMS/HHPA exhibited the highest weight loss in the second stage, suggesting lower thermal stability. It should be noted that the cured epoxy resin exhibited a first decomposition at a temperature lower than the decomposition temperatures of most OIHMs. Moreover, the major decrease in weight of OIHMs occurred over a broad range

of temperature rather than a drastic drop at a particular temperature, as observed in cured epoxy resin. The results indicate that the thermal stability of hybrid polymers was higher than that of the Si–O–C bond, with improved interaction between the organic and inorganic phases.

As observed from the TGA curves in Fig. 4, GPTMS/DETA illustrates a sharp drop in weight loss of 6.4 % at the temperature around 480 °C. A similar drastic drop of weight loss in TGA curves can also be seen from the previous studies [53, 54]. The cause of this phenomenon is still unknown. However, the weight loss in the temperature range of 400–500 °C is generally too high for organic compounds. Therefore, it was thought that the weight loss could be attributed to the degradation of unreacted GPTMS or a breakdown of GPTMS-derived product(s). More experimental results are required for a more complete understanding of this phenomenon.

3.3 DMTA studies

From Fig. 5, the storage modulus (E') of cured epoxy resin exhibited a drastic drop in the leathery region. The E' reached the lowest value of 463 MPa at a temperature around 100 °C, which indicates that the cured epoxy resin lost its stiffness by 85 %. On the other hand, the GPTMS/DETA hybrid material illustrated substantially higher thermal stability as E' remained stable in the rubbery plateau region. A similar trend could be seen for all OIHMs except for GPDMS/DETA. A decrease in E' was observed, which could be due to the lower cross-link density of the siloxane network as a result of difunctional GPDMS precursor. However, the drop in E' was gradual, whereas the drop in E' of cured epoxy resin was drastic. It is evident that the siloxane reinforced the epoxy in the hybrid polymer, although the inorganic component was linear siloxane chains, and the amount present in the GPDMS/DETA hybrid material was low.

It should be noted that the E' of GPTMS/DETA, GPTMS/AEAPTMS, GPTMS/HHPA, and GPDMS/HHPA increased slightly at temperatures above 100 °C. This could be explained by the further condensation reaction of silanol group. At a high temperature, the condensation reaction is driven toward completion. A higher E' value can be obtained as a result of extended inorganic network formation, which, in turn, increases the stiffness of the material [55].

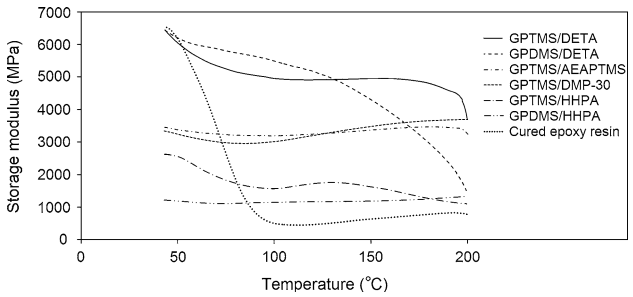

Fig. 5 Storage modulus (E') of OIHMs in comparison with the E' of cured epoxy resin

Cross-link density is the most important of a thermoset network as it influences strength and toughness of the material to some extent, as well as other properties such as free volume or diffusion coefficients for low molecular weight penetrants [55–57]. The value is often expressed as a number (or number of moles) of cross-links per unit volume or per unit mass [58]. The cross-link density of highly cross-linked thermoset coatings or thin films can be determined by modulus measurements at a temperature on the rubbery plateau. When the deformation of the sample is accommodated for by conformational changes, without bending or breaking of bonds, the relationship between rubbery plateau modulus and cross-link density can be determined as:

$$\nu_e = \frac{E'}{3RT}$$

where ν_e is the number of moles of elastically effective network chains per volume (mol m^{-3}), E' is the elastic modulus determined at a temperature above T_g (Pa), T is the absolute temperature corresponding to the E' value (K), and R is the universal gas constant (J K^{-1} mol^{-1}) [59, 60]. Cross-link densities of the OIHMs are summarized in Table 3. The E' values used in this calculation were taken from the modulus measurement at 150 °C (423 K), which is the temperature where the hybrid materials exhibited the rubbery plateau. R is the universal gas constant which is 8.314472 cm^{-1} MPa K^{-1} mol^{-1}.

The results showed that GPTMS/DETA had the highest cross-link density, and cured epoxy resin had the lowest value. It was observed that the cross-link density of GPTMS/DETA was higher than that of GPDMS/DETA. This result is in agreement with the results from FTIR spectra, which suggested that GPDMS/DETA is composed of an inorganic network with a lower cross-link density due to linear siloxane formation. The same trend can be observed in the OIHM of GPDMS/HHPA, in which the cross-link density was lower than that of GPTMS/HHPA. The OIHM of GPTMS/DMP-30 exhibited a slightly higher cross-link density compared to GPDMS/DETA despite having three-dimensional inorganic network in the hybrid material. This could be due to the organic network structure which is composed of linear poly(ethylene oxide), resulting in more steric hindrance generated in the OIHMs. In comparison with GPTMS/DMP-30, the cross-link density of GPTMS/HHPA was much lower. This could be explained by the higher content of linear siloxane chains

Table 3 Cross-link density and glass transition temperature (T_g) of OIHMs in comparison with the cured epoxy resin

Sample	E' (MPa)	T (K)	v_e (mol cm^3)	T_g (°C)
Cured epoxy resin	637	423	6.4×10^{-2}	86
GPTMS/DETA	4950	423	4.7×10^{-1}	110
GPDMS/DETA	3518	423	3.0×10^{-1}	108
GPTMS/AEAPTMS	4275	423	4.0×10^{-1}	Not detected
GPTMS/DMP-30	3457	423	3.3×10^{-1}	Not detected
GPTMS/HHPA	1459	423	1.4×10^{-1}	Not detected
GPDMS/HHPA	1082	423	1.0×10^{-1}	Not detected

that were found in GPTMS/HHPA hybrid material as a result of one-step acid-catalyzed sol–gel process. The high cross-link density of GPTMS/DMP-30 is due to the synthesis via acid–base-catalyzed sol–gel process in which the derived OIHM mainly composed of three-dimensional siloxane network.

Tan δ is related to the distribution of relaxation times of a polymer within a hybrid material. For OIHMs containing a high content of organic material, tan δ peaks are much broader than those of a neat organic polymer, but T_g can be identified [13]. From Fig. 6, the tan δ peak of GPTMS/DETA and GPTMS/AEAPTMS shifted to a higher temperature while it weakened and broadened compared to that of the cured epoxy resin (Fig. 7). Only T_g of GPTMS/DETA and GPTMS/AEAPTMS hybrid materials could be identified. The maximum tan δ of the other hybrid polymers (not shown) did not appear clearly during the material transition from brittle state to rubbery state (T_g). The tan δ peak of cured epoxy resin appeared at 68 °C, while the T_g of GPTMS/DETA and GPTMS/AEAPTMS appeared at 110 and 108 °C, respectively. It is well known that the decrease in modulus in the T_g region of a polymer is due to the Brownian motion of the network chains. The tan δ curves of both OIHMs showed that the micro-Brownian motion of the epoxy network was severely restricted by the interaction developed between the organic and inorganic components. The results confirm that the cross-links in hybrid polymers are covalently bonded rather than representing physical entangled macromolecular chains. The plateau observed in the storage modulus above T_g and the

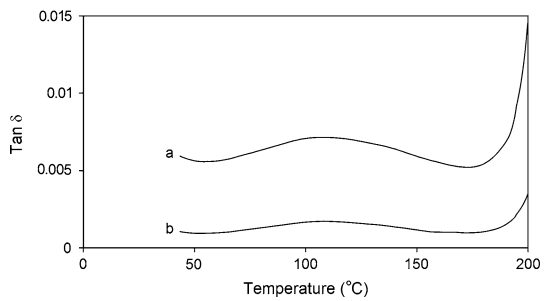

Fig. 6 Tan δ of *a* GPTMS/DETA and *b* GPTMS/AEAPTMS

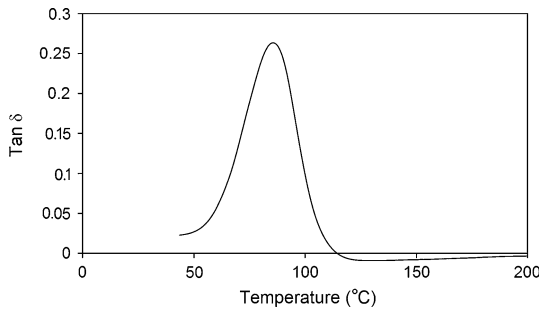

Fig. 7 Tan δ of cured epoxy resin

shift in T_g to a higher temperature are an indication of a high degree of cross-linking in both hybrid materials.

In general, δ ranges between 0° and 90°. As δ approaches 0°, the material exhibits purely elastic behavior. As δ approaches 90°, the material shows a purely viscous behavior. The OIHMs exhibited significant lower magnitude of tan δ, and the δ angle was close to 0° compared to that of cured epoxy resin [55]. This means the organic phase in the OIHMs exhibited elastic behavior, whereas the neat epoxy resin exhibited the behavior of a viscous fluid.

3.4 Solid-state NMR

Among a number of nuclei obtained from the NMR spectra, ^{29}Si and ^{13}C are the two most important nuclei for the characterization of the hybrid materials. The ^{29}Si and ^{13}C nuclei can be used to determine the level of polycondensation at silicon in the inorganic entity and the completion of epoxy ring-opening reaction, respectively. In the sol–gel process of an organosilane, the Si atom is bonded at least to one atom of carbon, and the four types of polycondensation can be described as T^1, T^2, T^3, and T^0 in which T^0 is corresponding to uncondensed species (Fig. 8; [61]). Similar to T species, silicon atom with the substitution by two carbon atoms can be easily identified in the case of OIHMs derived from difunctional organosilanes. The chemical shifts of these ^{29}Si NMR signals are described as D^0, D^1, and D^2.

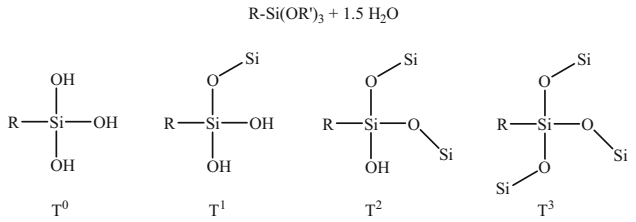

Fig. 8 Structure of alkyltrisilanol (T^0) and corresponding T^1, T^2, and T^3 polycondensation species

The ^{29}Si NMR of GPTMS/DETA and GPTMS/AEAPTMS showed two signals at approximately −59 ppm and −67 ppm with similar intensities (Fig. 9; [14, 15, 62]). These peaks can be assigned to T^2 and T^3 species corresponding to R–Si(OSi)$_2$OH and R–Si(OSi)$_3$ polycondensation species. The result is in good agreement with the FTIR result which indicates that the condensation of silanol groups was not completed as, in principle, the GPTMS precursor can form 100 % T^3 species. The NMR signal showed that the inorganic network of GPTMS/DETA contained a significant amount of Si–OH. However, it is well known that in practice the polycondensation of silicon is hardly ever complete although all of the precursor molecules have been [61]. For both OIHMs, there was no evidence of any peaks associated with T^1 and T^0 species, indicating that the condensation reaction of silanol groups proceeded toward completion.

From Fig. 9c, it can be seen that the OIHM of GPTMS/DMP-30 comprised mainly T^3 species with only a small portion of T^2 species. Furthermore, the ^{29}Si NMR resonance of GPTMS/DMP-30 also confirms that most of the hydroxyl groups in the material were from hydroxyl terminated poly(ethylene oxide) rather than the unreacted silanol groups. It was thought that the organic component of GPTMS/DMP-30 comprised short chains of poly(-ethylene oxide).

For the OIHM of GPTMS/HHPA, the ^{29}Si NMR signals showed that the T^2 species was dominant in the inorganic network (Fig. 9d). The result confirms that the OIHM derived from the acid-catalyzed sol–gel process contains a large portion of linear siloxane chains rather than a three-dimensional siloxane network. This is because the condensation reaction of silanol groups proceeds faster under basic catalysis [63]. The condensation reaction in the OIHMs derived from DETA, AEAPTMS, and DMP-30, therefore, yielded a higher content of T^3 species.

For OIHMs derived from difunctional organosilane, the chemical shifts are noticeably different from the

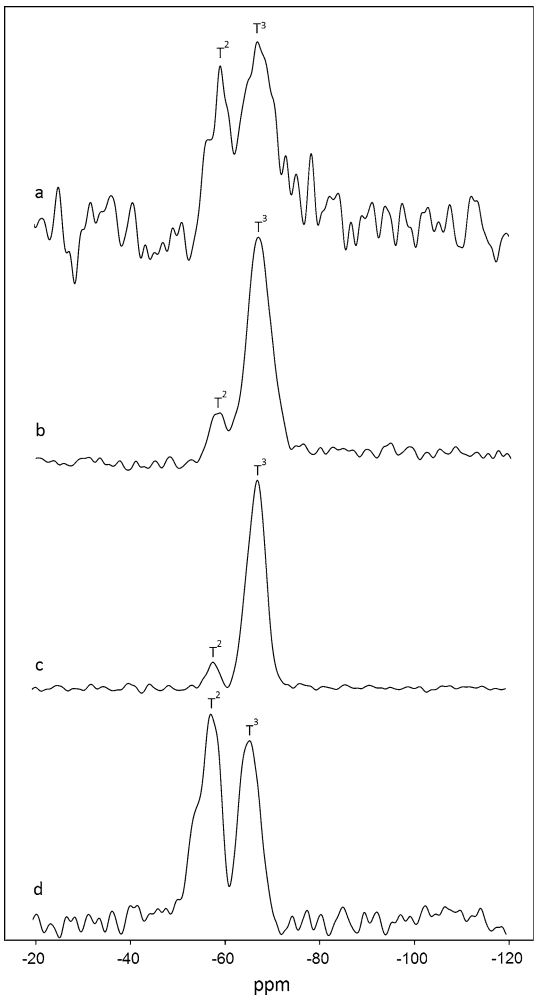

Fig. 9 ^{29}Si NMR spectrum of *a* GPTMS/DETA, *b* GPTMS/AEAPTMS, *c* GPTMS/DMP-30, and *d* GPTMS/HHPA hybrid materials

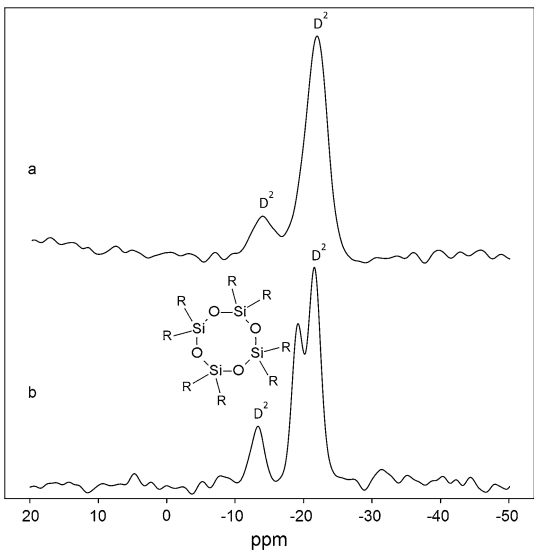

Fig. 10 ^{29}Si NMR spectrum of *a* GPDMS/DETA and GPDMS/HHPA hybrid materials

chemical shifts of the OIHM derived from trifunctional organosilane. The chemical shifts of ^{29}Si were observed in the region of −10 to −30 ppm. From Fig. 10, a minor peak appeared at −14 ppm can be assigned to disubstituted siloxane oligomers ($R_2Si(OSi)_2$) [64]. The major peak at −22 ppm is due to linear polysiloxane chains $(R_2SiO)_x$. It should be noted that both two peaks are D^2 species, but the peak at −22 ppm is the resonance of siloxane structure similar to silicone oil, which was composed of linear polysiloxane with disubstitution [65]. The result suggested that the inorganic network of GPDMS/DETA comprised mostly linear polysiloxane chains with a fraction of siloxane oligomers. This is in agreement with the FTIR results, in which the absorption peaks at 1080, 1052, and 1018 cm^{-1} indicate that the absorption of the siloxane is similar to that of polydimethylsiloxane.

Similar to GPDMS/DETA, the resonances of the siloxane appeared at −13 and −21 ppm. It is evident that the inorganic component of the OIHM contained a larger amount of disubstituted siloxane oligomers ($R_2Si(OSi)_2$) compared to that of GPDMS/DETA. The ^{29}Si NMR signals of GPDMS/HHPA also showed an extra peak at around −19 ppm, which could be attributed to octaalkylcyclotetrasiloxane $(R_2SiO)_4$ [65]. The structure of this siloxane species is shown in Fig. 10b. The result indicates that the inorganic network of GPDMS/HHPA contained a substantial amount of this cyclic species. This could be explained by the one-step acid-catalyzed sol–gel process of the difunctional organosilane.

4 Conclusion

The sol–gel process and the epoxy ring-opening reaction of GPTMS organosilane allowed the formation of organic–inorganic hybrid materials to be achieved. In this work, FTIR and NMR studies showed that siloxane network structures of the derived hybrid polymers depended greatly on the organosilane precursors and the epoxy curing agents. These parameters dictated the physical and thermomechanical properties of the materials as demonstrated by DMTA. It was evident that the presence of inorganic networks provided a significant improvement to the storage modulus of the hybrid materials typically increasing up to nearly eight times over the neat epoxy resin. An increase in the glass transition temperature, the end-use temperature, and the thermomechanical behavior of OIHMs was also observed and quantified. These results confirmed the feasibility of OIHMs used as replacements for diglycidyl ether of bisphenol-A (DGEBA) in the fabrication of composites for use at elevated temperatures.

Acknowledgments Manatchanok Sitthiracha would like to gratefully acknowledge Ministry of Science and Innovation (NZ) for financial support.

References

1. Ratna D (2005) Epoxy composites: impact resistance and flame retardancy. Rapra Technology Ltd, Shrewsbury
2. Hyer MW (2009) Stress analysis of fiber-reinforced composite materials. DEStech Publications Inc, Pensylvania
3. Park SJ, Seo MK (2011) Interface Sci Technol 18:501–629
4. Bunsell AR, Renard J (2005) Fundamentals of fibre reinforced composite materials. Institute of Physics Publishing, Bristol
5. Gull VE (1996) Structure and properties of conducting polymer composites. VSP BV, The Netherlands
6. Landry CJT, Coltrain BK, Wesson JA, Zumbulyadis N (1992) Polymer 33:1496–1506
7. Landry CJT, Coltrain BK, Brady BK (1992) Polymer 33:1486
8. Pathak SS, Khanna AS (2008) Prog Org Coat 62:409–416
9. Ershad-Langroudi A, Gharazi S, Rahimi A, Ghasemi D (2009) App Surf Sci 255:5746–5754
10. Philipp G, Schmidt H (1984) J Non Cryst Solids 63:283–292
11. Winkler RP, Arpac E, Schirra H, Sepeur S, Wegner I, Schmidt H (1999) Thin Solid Film 351:209–211
12. Arkles B (2001) MRS Bull 26:402–408
13. Gireesh KB, Jena KK, Allauddin S, Radhika KR, Narayan R, Raju KVSN (2010) Prog Org Coat 68:165–172
14. Donley MS, Mantz RA, Khramov AN, Balbyshev VN, Kasten LS, Gaspar DJ (2003) Prog Org Coat 47:401–415
15. Davis SR, Brough AR, Atkinson A (2003) J Non Cryst Solids 315:197–205
16. Chattopadhyay DK, Mishra AK, Sreedhar B, Raju KVSN (2006) Polym Degrad Stab 91:1837–1849
17. Innocenzi P, Sassi A, Brusatin G, Guglielmi M, Favretto D, Bertani R, Venzo A, Babonneau F (2001) Chem Mater 13: 3635–3643
18. Guglielmi M, Brusatin G, Della Giustina G (2007) J Non Cryst Solids 353:1681–1687
19. Sakka S, Yoko T (1992) In: Reisfeld R, Jørgensen CK (eds) Chemistry, spectroscopy and applications of sol–gel glasses. Springer, Germany
20. Shen S, Sun P, Li W, Parikh AN, Hu D (2010) Langmuir 26:7708–7716
21. Shajesh P, Smitha S, Aravind PR, Warrier KGK (2009) J Colloid Interface Sci 336:691–697
22. Innocenzi P, Esposto M, Maddalena A (2001) J Sol–Gel Sci Technol 20:293–301
23. Fu S, Wu P, Han Z (2002) Compos Sci Technol 62:3–8
24. Mammeri F, Bourhis EL, Rozes L, Sanchez C (2005) J Mater Chem 15:3787–3811
25. Malzbender J, den Toonder JMJ, Balkenende AR, de With G (2002) Mater Sci Eng 36:47–48
26. Mammeri F, Rozes L, Sanchez C (2003) J Sol–Gel Sci Technol 26:413–417
27. Thermal Analysis: Measurement of T_g by DSC (2013) Perkin Elmer. http://www.perkinelmer.com. Accessed 19 July 2013
28. Menczel JD, Prime RB (2009) Thermal analysis of polymers. Wiley, New Jersey
29. Hare CH (1998) Protective coating: fundamental of chemistry and composition. The Society for Protective Coating, USA
30. Mileca CA, Bogatu C, Duţă A (2011) Bulletin of the Transylvania University of Braşov. Transylvania University Press, Transylvania

31. Chen WY, Wang YZ, Kuo SW, Huang CF, Tung PH, Chang FC (2004) Polym 45:6897–6908
32. Sánchez-Soto M, Pagés P, Lacorte T, Briceño K, Carrasco F (2007) Compos Sci Technol 67:1974–1985
33. Brinker CJ, Sherer GW (1985) J Non Cryst Solids 70:301–322
34. Bourget L, Corriu RJP, Leclercq D, Mutin PH, Vioux A (1998) J Non Cryst Solids 242:81–91
35. Saunders KJ (1973) Organic polymer chemistry: an introduction to the organic chemistry of adhesives, fibres, paints, plastics, and rubbers. Redwood Press Ltd, Great Britain
36. Lam JCK, Huang MYM, Tan H, Mo Z, Mai Z (2011) J Vac Sci Technol A 29(5):0515131–0515136
37. Rauter A, Perše LS, Orel B, Bengű B, Sunetci O, Vuk AS (2013) J Electroanal Chem 703:97–107
38. Launer PJ (1987) In: Arkels B (ed) Silicone compounds register and review. Petrarch Systems, Pennsylvania
39. Jing SY, Lee HJ, Choi CK (2002) J Korean Phys Soc 41:769–773
40. Davidovits J (2005) Geopolymer green chemistry and sustainable development solutions. Institut Géopolymère, France
41. Ni L, Moreau N, Chemtob A, Croutxé-Barghorn C (2012) J Sol–Gel Sci Technol 64(2):500–509
42. Chemtob A, Peter M, Belon C, Dietlin C, Croutxé-Barghorn C, Vidal L, Rigolet S (2010) J Mater Chem 20:9104–9112
43. Gardin S, Bozio R, Brusatin G, Della Giustina G, Giorgetti E, Guglielmi M, Signorini R (2006) Proc SPIE 6192:321–329
44. Anastassopoulou JD (1991) In: Rizzarelli E, Theophanides T (eds) Chemistry and properties of biomolecular systems. Springer, Berlin
45. Ahn D, Jeong YC, Lee S, Lee J, Heo Y, Park JK (2009) Opt Express 17:16603–16612
46. Bistričić L, Borjanović V, Mikac L, Dananić V (2013) Vib Spectrosc 68:1–10
47. Frampton MB, Séguin JP, Marquardt D, Harroun TA, Aelisko PM (2013) J Mol Catal B Enzym 85–86:149–155
48. Mao Z, Yan CQ (2000) J Appl Polym Sci 81:2142–2150
49. Gao A, Zhao Z, Ou Y, Qi A, Wang F (1996) Polym Int 40:187–192
50. Wei Y, Bakthavatchalam R, Yang D, Whitecar CK (1991) Polym Prepr (Am Chem Soc, Div Polym Chem) 32:503
51. Liu J, Xu T, Gong M, Fu Y (2005) J Membr Sci 264:87–96
52. Liu J, Xu T, Fu Y (2005) J Non Cryst Solids 351:3050–3059
53. Gizdavic-Nikolaidis MR, Edmonds NR, Bolt CJ, Easteal AJ (2008) Curr App Phys 8:300–303
54. Guo R, Hu C, Pan F, Wu H, Jiang Z (2006) J Membr Sci 281:454–462
55. Mammeri F, Le Bourhis E, Rozes L, Sanchez C (2005) J Mater Chem 15:3792–3795
56. Ochi M, Takahashi R (2001) J Polym Sci Part B Polym Phys 39:1071–1084
57. Kaiser T (1989) Prog Polym Sci 14:408
58. Boveri AB (1989) Prog Polym Sci 14:373–450
59. Hill LW (1997) Prog Org Coat 31:235–243
60. (2007) Pigment & Resin Technology. doi:10.1108/prt.2007.12936ead.001
61. Corriu R, Anh NT (2009) Molecular chemistry of sol–gel derived nanomaterials. Wiley, UK
62. Alonso B, Massiot D, Valentini M, Kidchob T, Innocenzi P (2008) J Non Cryst Solids 354:1618
63. Brinker CJ, Scherer GW (1991) Sol–gel science: the physics and chemistry of sol–gel processing. Academic Press, California
64. Bein T, Carver RF, Farlee RD, Stucky GD (1988) J Am Chem Soc 110:4546–4553
65. ^{29}Si NMR some practical aspects (2003). Gelest 208–222. http://www.pascal-man.com/periodic-table/29Si.pdf. Accessed 2 June 2014